

# Experimental characterization of the stagnation layer between two obliquely merging supersonic plasma jets

E. C. Merritt,<sup>1,2</sup> A. L. Moser,<sup>1</sup> S. C. Hsu,<sup>1,\*</sup> J. Loverich,<sup>3</sup> and M. Gilmore<sup>2</sup>

<sup>1</sup>*Los Alamos National Laboratory, Los Alamos, NM, 87545, USA*

<sup>2</sup>*University of New Mexico, Albuquerque, NM, 87131, USA*

<sup>3</sup>*Tech-X Corporation, Boulder, CO, 80303, USA*

(Dated: March 11, 2019)

We present spatially resolved measurements characterizing the stagnation layer between two obliquely merging supersonic plasma jets. Intra-jet collisionality is very high ( $\lambda_{ii} \ll 1$  mm), but the inter-jet ion-ion mean free paths are on the same order as the stagnation layer thickness (a few cm). Fast-framing camera images show a double-peaked emission profile transverse to the stagnation layer, with the central emission dip consistent with a density dip observed in the interferometer data. We demonstrate that our observations are consistent with collisional oblique shocks.

Colliding plasmas have been studied in a variety of contexts, e.g., counterstreaming laser-produced plasmas supporting hohlraum design for indirect-drive inertial confinement fusion [1–3], forming and studying astrophysically relevant shocks [4–8], and for applications such as pulsed laser deposition [9] and laser induced breakdown spectroscopy [10]. Physics issues arising in these studies include plasma interpenetration [11–16], shock formation [17], and the formation and dynamics of a stagnation layer between the colliding plasmas [18–20]. In this work, we present experimental results of two obliquely merging supersonic plasma jets. These and other recent jet merging experiments [21, 22] were conducted to explore the feasibility of forming imploding spherical plasma liners via an array of merging plasma jets [23–27], which could have applications in forming cm-,  $\mu$ s-, and Mbar-scale plasmas for fundamental high energy density physics studies [28] and as a standoff driver for magnetoinertial fusion [23, 29–32]. Prior experiments studying the stagnation layer between colliding laser-produced or wire-array z-pinch [33] plasmas were on smaller spatial scales (mm or smaller) that could not be fully resolved by measurements. New results in the present work are the experimental identification and characterization of a few-cm thick stagnation layer between colliding plasmas, and the demonstration that our observations are consistent with hydrodynamic oblique shock theory [34].

Experiments reported here are conducted on the Plasma Liner Experiment (PLX) [35], in which two supersonic argon plasma jets are formed and launched by plasma railguns [36]. Plasma jet parameters at the exit of the railgun nozzle (peak  $n_e \approx 2 \times 10^{16}$  cm<sup>-3</sup>, peak  $T_e \approx 1.4$  eV,  $V_{jet} \approx 30$  km/s, Mach number  $M \equiv V_{jet}/C_{s,jet} \approx 14$ , diameter = 5 cm, and length  $\approx 20$  cm) and their evolution during subsequent jet propagation have been characterized in detail [35]. The jet magnetic field inside the railgun is  $\sim 3$  T, but the classical magnetic diffusion time is a few  $\mu$ s [35], and thus we ignore the effects of a magnetic field by the time of jet merging ( $> 20$   $\mu$ s). Experimental data are from

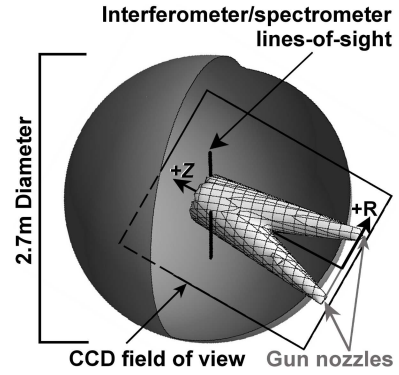


FIG. 1. Schematic of the experiment showing the spherical vacuum chamber, location of railgun nozzles mounted  $24^\circ$  apart, two obliquely merging plasma jets, ( $R, Z$ ) coordinates used in the paper, approximate interferometer/spectrometer lines-of-sight ( $Z \approx 84$  cm), and CCD camera field-of-view.

an eight-chord laser (561 nm) interferometer [37, 38], a visible-to-near-infrared 0.275 m survey spectrometer (600 lines/mm grating and 0.45  $\mu$ s gating on the 1024-pixel MCP array detector), and an intensified charge-coupled device (CCD) visible-imaging camera (DiCam Pro,  $1280 \times 1024$  pixels, 12-bit dynamic range). The interferometer and spectrometer chords intersect the merging jets at  $Z \approx 84$  cm (Fig. 1). Each interferometer probe beam has a diameter of  $\approx 3$  mm, and the chords are each separated by 1.5 cm transverse to the merge plane. The spectrometer has an  $\approx 7$  cm diameter field-of-view in the vicinity of the merge plane. More details about PLX, the railguns, diagnostics, and characterization of individual plasma jets are given elsewhere [35].

Figure 2 shows the time evolution of oblique jet-merging. Formation of a stagnation layer between the two jets and its double-peaked emission profile in the transverse ( $R$ ) direction are clearly visible. We made interferometer and spectrometer measurements of the stagnation layer at  $Z \approx 84$  cm (Fig. 3a) for the cases of top-only, bottom-only, and both jets firing. Figure 3b shows the interferometer phase shift  $\Delta\phi$  versus

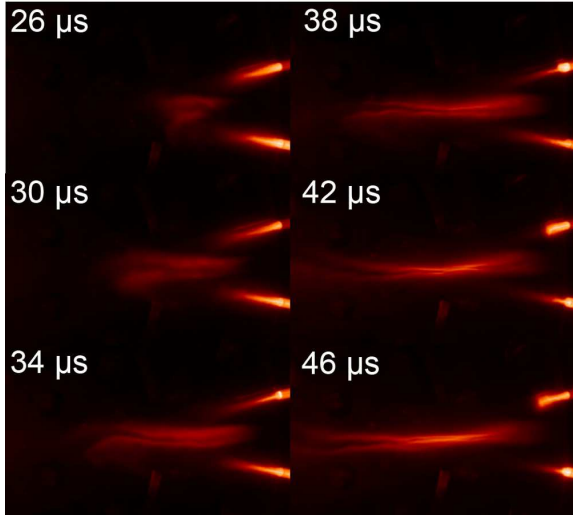


FIG. 2. False-color, slightly cropped, CCD images (log intensity, 20 ns exposure) of oblique jet-merging (shots 1130, 1128, 1125, 1120, 1134, 1138). The two railgun nozzles ( $\approx 46$  cm apart) are visible on the right-hand-side of each image.

time at the  $R = 2.25$  cm chord position for each case. Merged-jet measurements show that, at  $R = 2.25$  cm,  $\Delta\phi_{\text{merge}} > \Delta\phi_{\text{top}} + \Delta\phi_{\text{bottom}}$  (Fig. 3b), implying that simple jet interpenetration cannot account for the observed  $\Delta\phi$  of the merged-jet stagnation layer (more quantitative analysis given later). However, at large  $R$  (e.g., 6.75 cm),  $\Delta\phi_{\text{merge}} \approx \Delta\phi_{\text{top}} + \Delta\phi_{\text{bottom}}$  (not shown), consistent with jet interpenetration. Figure 3c shows  $\Delta\phi$  vs.  $R$  at four times for a merged jet. The  $\Delta\phi$  dip at  $R = 0.75$  cm and peak at  $R = 2.25$ –4 cm are well-aligned with the emission dip and peak (Fig. 3a), respectively.

The interferometer  $\Delta\phi$  measurements are used to estimate the ion plus neutral density  $n_{\text{tot}}$ . Our interferometer is sensitive to bound and free electrons in the plasma [38], so  $\Delta\phi$  contributions from all species and ionization states must be considered. The  $\Delta\phi$  satisfies  $\int n_{\text{tot}} dl = \frac{\Delta\phi}{C_e [Z_{\text{eff}} - \text{Err}]}$ , where the integral is over the chord length,  $C_e = \lambda e^2 / 4\pi\epsilon_0 m_e c^2$  is the phase sensitivity to electrons,  $Z_{\text{eff}} = n_e / n_{\text{tot}}$  is the mean charge,  $\text{Err} = \sum_{j,k} (2\pi / \lambda C_e n_{\text{tot}}) K_{j,k} m_k n_{j,k}$  is the error in the phase shift due to all ionization states  $j$  of all ion species  $k$ ,  $m_k$  is the atomic mass of ion species  $k$ , and  $K_{j,k}$  is the specific refractivity. Uncertainty in plasma jet composition (due to impurities) can be accounted for by bounding  $n_{\text{tot}}$  at the extremes  $\text{Err} = 0$  and  $\text{Err} = \text{Err}_{\text{max}} = (2\pi m / \lambda C_e) K_{\text{max}}$ , where  $K_{\text{max}}$  is the largest specific refractivity of all the species present. Since we do not know precisely the impurity fraction or mixture ratios of impurities, we perform our data analysis by considering two extreme cases of (i) 100% argon and (ii) 30% argon with 70% impurities. The latter is chosen based on the difference in measured chamber pressure rise for gas-injection-only versus full plasma discharges. Iden-

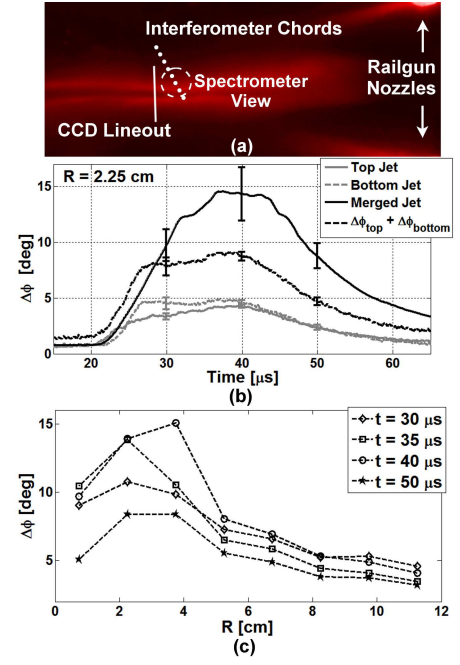


FIG. 3. (a) CCD line-out, interferometer chord positions, and spectrometer view overlaid on a CCD image ( $t = 38$  μs). (b) Multi-shot averaged interferometer phase shift vs. time at  $R = 2.25$  cm. (c) Phase shift vs. chord position for a jet-merging case (shot 1120).

tification of bright Al and O spectral lines in our data suggest that impurities are from the alumina-based railgun insulators. Thus, for case (ii), we approximate the plasma jet to be 43% O and 24% Al and assume that  $\text{Err}_{\text{max}} = \text{Err}_{\text{Al I}}$ . Top-jet-only experiments provide single-jet  $\Delta\phi$  vs. time at  $Z \approx 84$  cm and  $R = 2.25$  cm (Fig. 3b). The average single-jet peak phase shift is  $\Delta\phi = 4.3 \pm 0.3^\circ$  for the data considered (shots 1265–1267). All chord positions  $R = 0.75$ –11.25 cm (Fig. 3a) have similar  $\Delta\phi \approx 4^\circ$ . Using  $\Delta\phi = 4^\circ$ ,  $Z_{\text{eff}} = 0.94$  (inferred from spectroscopy analysis [35] assuming 100% argon),  $\text{Err}_{\text{max}} = 0.082$ , and a jet diameter of 22 cm (from CCD images [35]), gives a single-jet density range of  $n_{\text{tot}} = n_{\text{single}} = 2.1$ – $2.3 \times 10^{14}$  cm $^{-3}$ . The latter result changes by only a few percent for the 30%/70% mixture, which changes the inferred  $Z_{\text{eff}}$  to 0.92.

By using the interferometry estimates for merged-jet density (shown later) and comparing our spectroscopy data with non-LTE spectral calculations using PrismSPECT [39], we infer  $Z_{\text{eff}}$  and  $T_e$  of the stagnation layer at  $Z \approx 84$  cm. PrismSPECT results for  $Z_{\text{eff}}$  and  $T_e$  are sensitive to the specific plasma mixture used. Based on the presence of certain Ar II lines in the data and by comparing to PrismSPECT results, we bound estimates of  $Z_{\text{eff}}$  and  $T_e$  using the 100% argon and 30%/70% mixture cases. For the former (Fig. 4a), we infer that peak  $T_e \geq 1.4$  eV and  $Z_{\text{eff}} = 0.94$ . For the latter (Fig. 4b), we infer that  $2.2$  eV  $\leq$  peak  $T_e < 2.3$  eV and  $Z_{\text{eff}} = 1.3$ –1.4,

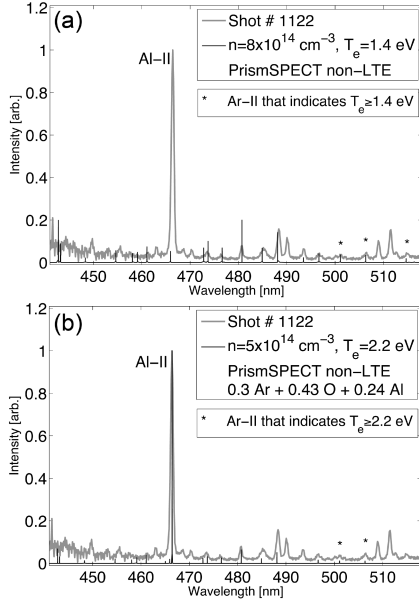


FIG. 4. Spectral data (gray) and non-LTE PrismsPECT calculations (black) for the merged-jet stagnation layer ( $Z \approx 84$  cm,  $t = 36$   $\mu$ s). The PrismsPECT calculations are for (a) 100% argon and (b) 30%/70% mixture. Lower bounds on peak  $T_e$  are inferred based on the presence of the Ar II lines indicated by asterisks.

with the upper bounds determined by the absence of an Al III line in the data. For the mixture,  $M \approx 9$  compared to  $M \approx 14$  for pure argon.

With estimates of the stagnation layer  $Z_{\text{eff}}$  in hand, we estimate the stagnation layer density and compare it with the single-jet (un-shocked) density. At  $R = 2.25$  cm, the average peak  $\Delta\phi = 14.3 \pm 2.4^\circ$  (Fig. 3b) (shots 1117–1196). Using  $\Delta\phi = 14^\circ$ , chord path length of 22 cm, and  $Z_{\text{eff}} = 0.94$  (100% argon case),  $n_{\text{tot}} = n_{\text{merged}} = 7.5\text{--}8.2 \times 10^{14}$   $\text{cm}^{-3}$ . In this case the density increase  $n_{\text{merged}}/n_{\text{single}} = 3.2\text{--}3.8$ . For  $Z_{\text{eff}} = 1.4$  (30%/70% mixture case), the stagnation layer density is  $n_{\text{tot}} = n_{\text{merged}} = 5.0\text{--}5.3 \times 10^{14}$   $\text{cm}^{-3}$ , and the density increase is  $n_{\text{merged}}/n_{\text{single}} = 2.1\text{--}2.5$ . Thus, the observed range of  $n_{\text{merged}}/n_{\text{single}} = 2.1\text{--}3.8$ , exceeding the factor of two expected for jet interpenetration.

We compare the experimentally inferred density jumps with oblique shock theory [34]. At  $Z \approx 84$  cm and  $M = 9\text{--}14$ , the theory predicts a shock angle  $\beta \approx 19^\circ\text{--}20^\circ$ , as discussed later. For  $\gamma = 1.4$ , the predicted density jump across an oblique shock [28] is  $n_{\text{shock}}/n_{\text{unshocked}} = (M \sin \beta)^2(\gamma+1)/[(M \sin \beta)^2(\gamma-1)-2] \approx 4.0\text{--}4.9$ . Difference between the measured and predicted density jumps could be due to 3D (e.g., pressure-relief in the out-of-page dimension) and/or equation-of-state (e.g., ionization [22]) effects not modeled by the theory.

The stagnation layer thicknesses as observed in the merged-jet emission (Fig. 5) and  $\Delta\phi$  vs.  $R$  profiles (Fig. 3c) are similar in scale (few cm). In a collisional

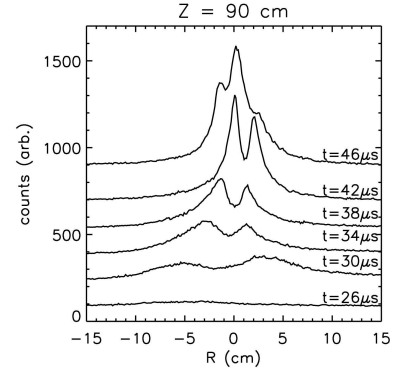


FIG. 5. CCD image line-outs versus  $R$  (transverse to stagnation layer) at  $Z = 90$  cm (horizontal pixel # 654 out of 1024), corresponding to the images of Fig. 2. Progressive times are shown with increasing count offsets to avoid trace overlap.

plasma, the layer thickness is expected [14] to be of order the counter-streaming ion-ion mean free path (mfp)  $\lambda_{ii'} \sim v_{\text{rel}}/4\nu_{ii'}$  [22], where  $v_{\text{rel}}$  is the relative transverse velocity between obliquely merging jets and the slowing-down rate in the fast approximation ( $v_{\text{rel}} \gg v_{ti}$ ) is  $\nu_{ii'} \approx 9.0 \times 10^{-8}(1/\mu + 1/\mu')(\mu^{1/2}/\epsilon^{3/2})n_{i'}(Z_{\text{eff}}Z'_{\text{eff}})^2 \ln \Lambda$  [40]. Note that in our parameter regime, the inter-jet  $\lambda_{ie} \gtrsim \lambda_{ii}$ . We estimate  $\lambda_{ii'}$  by considering jets of 100% argon and the 30%/70% mixture previously discussed, in all cases using  $v_{\text{rel}} = 20$  km/s. For Ar-Ar stopping,  $\lambda_{ii} = 3.47$  cm (for  $n_i = 8 \times 10^{14}$   $\text{cm}^{-3}$ ,  $T_e = 1.4$  eV,  $Z_{\text{eff}} = 0.94$ ). Pure Al-Al and O-O stopping yield  $\lambda_{ii} = 0.16$  and  $0.62$  cm, respectively (for  $n_i = 5 \times 10^{14}$   $\text{cm}^{-3}$ ,  $T_e = 2.2$  eV,  $Z_{\text{eff,Al}} = 2.0$ ,  $Z_{\text{eff,O}} = 1.0$ ). For inter-species collisions in a mixed-species jet, using the mixture given in Fig. 4b,  $\lambda_{ii'} \approx 0.57\text{--}6.18$  cm. We have also estimated the inter-jet mfp due to  $\text{Ar}^+\text{-Ar}$  charge-exchange and momentum transfer [41] to be  $\approx 3$  cm. These estimates imply that our inter-jet merging is in a collisional regime, which is consistent with a more detailed treatment of inter-jet ion-ion stopping including jet profile effects [22].

Assuming that the emission layers are post-shocked plasma, we postulate that their edges (at larger  $|R|$ ) are the shock boundaries (Fig. 6). Qualitatively, the merging geometry for an individual jet resembles that of a supersonic flow past a wedge [34] and should result in the formation of a linear attached shock at an angle  $\beta$  with respect to the original flow direction. The angle  $\beta$  is a function of  $M$  and the wedge angle  $\delta$  between the jet flow and the midplane, and satisfies  $\tan \delta = 2 \cot \beta \frac{M_1^2 \sin^2 \beta - 1}{M_1^2 (\gamma + \cos 2\beta) + 2}$  [34]. In our case,  $\tan \delta = (23 \text{ cm})/Z_i$ , where  $Z_i$  is the point at which jets first interact. We estimated  $Z_i$  from CCD images as the minimum  $Z$  for which merged-jet emission is observed, with  $Z_i \approx 45$  cm at  $t = 26$   $\mu$ s evolving to  $Z_i \approx 25$  cm at  $t = 46$   $\mu$ s. For this range of  $Z_i$ , we predict shock angles (relative to the midplane)  $\beta - \delta \approx 8^\circ\text{--}17^\circ$  ( $M = 9$ ) and  $7^\circ\text{--}15^\circ$  ( $M = 14$ ). For

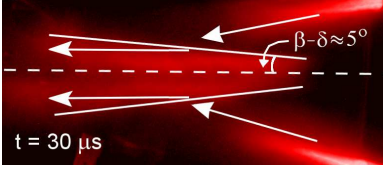


FIG. 6. CCD image (shot 1089,  $t = 30 \mu\text{s}$ ) with postulated shock boundaries (solid white lines) and observed shock angle  $\beta - \delta \approx 5^\circ$  relative to the midplane.

shot 1089 with  $Z_i \approx 30 \text{ cm}$ ,  $\beta - \delta \approx 5^\circ$  (Fig. 6), which is within a factor of two of the predicted  $\beta - \delta \approx 9^\circ - 10^\circ$ . This is reasonable given that the prediction does not include 3D nor equation-of-state [22] effects. Oblique shock theory also predicts the formation of a detached shock [34], which would have a curved shock boundary for  $\delta > \delta_{max} \approx 45^\circ$  (for  $M = 9-14$  and  $Z_i \approx 25 \text{ cm}$  at late times). CCD images at  $t \geq 42 \mu\text{s}$  (Fig. 2) show curvature of the emission layers away from the midplane, suggestive of detached shocks.

To further evaluate the consistency of the experimental results with oblique shock theory [34], we ran 1D multi-fluid simulations of merging jets, treating the electrons as one fluid and the ions of each jet as a second and third fluid. This models the transverse ( $R$ ) dynamics of the oblique merging. Simulations were performed with the multi-fluid magnetohydrodynamics code USim, formerly known as Nautilus [42]. In the simula-

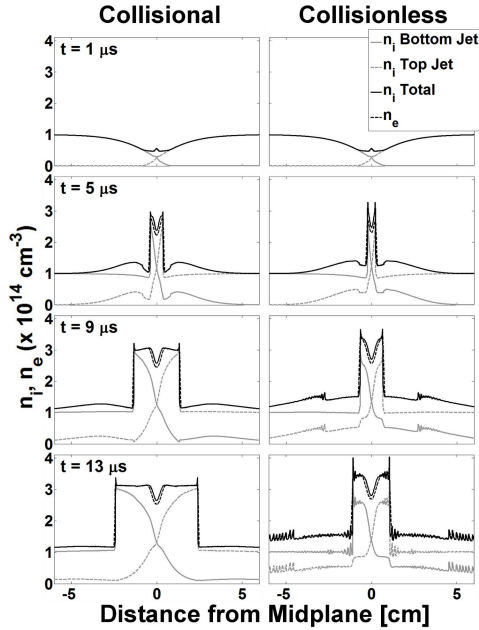


FIG. 7. Density versus spatial dimension from 1D multi-fluid collisional (left column) and collisionless (right column) plasma simulations that model the transverse ( $R$ ) dynamics of our experiments, illustrating the formation of reflected shocks in both cases.

tions, the jets are assumed to be 100% Ar II with initial  $n_e = n_i = 10^{14} \text{ cm}^{-3}$ ,  $T_e = T_i = 1.4 \text{ eV}$ , and velocities of  $\pm 6.2 \text{ km/s}$  (i.e., transverse component of  $V_{jet} \approx 30 \text{ km/s}$ ). We used a density profile in the leading edge of the jet as shown in the top panels of Fig. 7. We performed both collisional [14] and collisionless simulations with the same initial conditions to evaluate the differences between the two cases. The simulations have resolution  $\sim 100 \mu\text{m}$ , which does not resolve the Debye length ( $\lambda_D \sim 1.0 \mu\text{m}$ ). However, we verified the formation of an electrostatic collisionless shock on reduced density simulations that do resolve  $\lambda_D$ . Details of the semi-implicit numerical algorithm are described in [43]. At  $1 \mu\text{s}$  after merging begins, both collisionless and collisional simulations show a small initial density buildup at the merging interface. Within  $5 \mu\text{s}$ , a density dip appears at the midplane, similar to the structure seen for tens of microseconds in the experiments. At these jet parameters, the collisional and collisionless simulations give the same qualitative features, i.e., the multi-layer reflected shock structure that is consistent with the double-peaked emission seen in Fig. 2. Subtle differences between the collisional and collisionless simulation results, i.e., reflected shock speed and degree of ion interpenetration, cannot at present be resolved by the experimental data. The simulation results provide further support to the interpretation that our observations are consistent with collisional oblique shocks.

In summary, we have experimentally characterized the stagnation layer between two obliquely merging supersonic plasma jets. The jets are individually very highly collisional, but the inter-jet ion-ion collisional mean free path is of the same order as the stagnation layer thickness of a few centimeters. CCD images show the formation of a stagnation layer with a double-peaked emission profile transverse to the layer, with the central emission dip consistent with a density dip observed in the interferometer data. The overall geometry of the observed stagnation layer structure is consistent with hydrodynamic oblique shock theory. Furthermore, collisional 1D multi-fluid plasma simulations that model the transverse dynamics of the oblique merging show the formation and evolution of reflected shocks with a central density dip consistent with the observed stagnation layer. Ongoing experiments are now employing lower jet density and higher jet velocity to study head-on jet merging with very low inter-jet ion-ion collisionality.

We acknowledge J. Dunn for experimental support, S. Brockington and F. D. Witherspoon for advice on railgun operation, and C. Thoma and J. Cassibry for discussions regarding the simulations. This work was supported by the U.S. Dept. of Energy.

---

\* Electronic address: scotthsu@lanl.gov

- [1] R. A. Bosch *et al.*, Phys. Fluids **B4**, 979 (1992).
- [2] O. Rancu *et al.*, Phys. Rev. Lett. **75**, 3854 (1995).
- [3] A. S. Wan *et al.*, Phys. Rev. E **55**, 6293 (1997).
- [4] N. C. Woolsey *et al.*, Phys. Plasmas **8** (2001).
- [5] L. Romagnani *et al.*, Phys. Rev. Lett. **101**, 025004 (2008).
- [6] Y. Kuramitsu *et al.*, Phys. Rev. Lett. **106**, 175002 (2011).
- [7] N. Kugland *et al.*, Nature Phys. **8**, 809 (2012).
- [8] J. S. Ross *et al.*, Phys. Plasmas **19**, 056501 (2012).
- [9] H. Luna *et al.*, J. Appl. Phys. **101**, 033302 (2007).
- [10] C. Sánchez-Aké *et al.*, Spectrochimica Acta B **65**, 401 (2010).
- [11] R. L. Berger *et al.*, Phys. Fluids **B3**, 3 (1991).
- [12] S. M. Pollaine, R. L. Berger, and C. J. Keane, Phys. Fluids B **4**, 989 (1992).
- [13] O. Larroche, Phys. Fluids B **5**, 2816 (1993).
- [14] P. W. Rambo and J. Denavit, Phys. Plasmas **1**, 4050 (1994).
- [15] P. W. Rambo and R. J. Procassini, Phys. Plasmas **2**, 3130 (1995).
- [16] M. Jones *et al.*, Phys. Plasmas **3**, 1096 (1996).
- [17] M. Y. Jaffrin and R. F. Probst, Phys. Fluids **7**, 1658 (1964).
- [18] P. Hough *et al.*, J. Phys. D: Appl. Phys. **42**, 055211 (2009).
- [19] P. Hough *et al.*, J. Appl. Phys. **107**, 024904 (2010).
- [20] P. Yeates *et al.*, Phys. Plasmas **18** (2011).
- [21] A. Case *et al.*, Phys. Plasmas **20**, 012704 (2013).
- [22] S. Messer *et al.*, Phys. Plasmas **20**, 032306 (2013).
- [23] P. B. Parks, Phys. Plasmas **15**, 062506 (2008).
- [24] T. Awe *et al.*, Phys. Plasmas **18**, 072705 (2011).
- [25] J. S. Davis *et al.*, Phys. Plasmas **19**, 102701 (2012).
- [26] J. T. Cassibry *et al.*, Phys. Plasmas **19**, 052702 (2012).
- [27] J. T. Cassibry, M. Stanic, and S. C. Hsu, Phys. Plasmas **20**, 032706 (2013).
- [28] R. P. Drake, *High-Energy-Density-Physics* (Springer-Verlag, Berlin, 2006).
- [29] Y. C. F. Thio *et al.*, in *Current Trends in International Fusion Research—Proceedings of the Second International Symposium*, edited by E. Panarella (NRC Canada, Ottawa, 1999).
- [30] S. C. Hsu *et al.*, IEEE Trans. Plasma Sci. **40**, 1287 (2012).
- [31] J. F. Santarius, Phys. Plasmas **19**, 072705 (2012).
- [32] H. Kim *et al.*, Phys. Plasmas **20**, 022704 (2013).
- [33] G. F. Swadling *et al.*, Phys. Plasmas **20**, 022705 (2013).
- [34] L. D. Landau and E. M. Lifshitz, *Fluid Mechanics 2nd Ed.*, Vol. 6 (Butterworth-Heinemann, 2011) pp. 313–350.
- [35] S. C. Hsu *et al.*, Phys. Plasmas **19**, 123514 (2012).
- [36] F. D. Witherspoon *et al.*, Bull. Amer. Phys. Soc **56**, 311 (2011).
- [37] E. C. Merritt *et al.*, Rev. Sci. Instrum. **83**, 033506 (2012).
- [38] E. C. Merritt *et al.*, Rev. Sci. Instrum. **83**, 10D523 (2012).
- [39] J. J. MacFarlane *et al.*, in *Inertial Fusion Sciences and Applications 2003*, edited by B. A. Hammel, D. D. Meyerhofer, and J. Meyer-ter-Vehn (American Nuclear Society, 2004) p. 457.
- [40] J. D. Huba, *NRL Plasma Formulary*, 2011, p. 32.
- [41] A. V. Phelps, J. Phys. Chem. Ref. Data **20**, 557 (1990).
- [42] J. Loverich and A. Hakim, J. Fusion Energy **29**, 532 (2010).
- [43] H. Kumar and S. Mishra, J. Sci. Comput. **52**, 401 (2012).